The non-uniformity of CCDs and the effects of spatial undersampling.

Paul R. Jorden, Jean-Marc Deltorn (*), A P Oates.

Royal Greenwich Observatory
Madingley Road,
Cambridge
CB3 0EZ, UK

(* Normal address, ENSPG, Grenoble)

ABSTRACT

CCDs are widely used in astronomy for spectroscopy, photometry, astrometry, and many other applications. This array sensor has a periodic structure which defines individual picture elements (pixels). The stability and excellent overall response of this type of detector are well known. Less widely described is the fact that the internal structure of the array gives rise to intra-pixel variations in responsivity. These response modulations are particularly relevant when the data is spatially undersampled- a situation that is not entirely uncommon in certain instruments.

We have made detailed measurements of the response variations within CCDs, using an experimental arrangement that gave a 2 micron resolution. Optical response has been determined at all sample points within a pixel, at selected wavelengths in the range 400-900 nm. Measurements are presented for front-illuminated thick (EEV) devices and backside-illuminated thin (Tek) CCDs. Models of the internal structure have been constructed, and used to calculate theoretical response data; these have been compared with the experimental results. An example of an extracted (FOS) spectrum which demonstrates these undersampling effects is discussed.

1. INTRODUCTION

In many observatories, including ours, the CCD is now the most important type of optical sensor and at RGO we have characterised and installed many such devices for use on our telescopes (at the international Roque de los Muchachos Observatory in La Palma). Most attention has been paid to parameters such as readout noise, charge-transfer, and global quantum efficiency. However, prompted by some recent discussions about sampling effects and data extraction, we have now looked in more detail at the internal structure of the CCD, and measured response modulation on sub-pixel spatial scales. Intra-pixel non-uniformity has been examined previously by Purll (1978) and Wright (1982), but neither authors studied recently-made high-quality CCDs, or examined the effects over a range of wavelengths with the precision that we have achieved.

In this paper we describe the nature of our experimental arrangements, and then detail the systematic measurements of intra-pixel response for several types of CCD. We have examined three different types of CCD, all of which have been used on our telescopes. The results are presented, and compared with models of the CCD structure; most of the observed effects can be explained although a few were not expected. With this knowledge of intra-pixel response, we are then able to discuss some actual (undersampled) spectra and explain the results obtained.

2. THE EXPERIMENTAL ARRANGEMENT.

2.1 Introduction

In order to study the intra-pixel sensitivity structure of the CCD, we arranged to project a very small light spot onto the CCD. A demagnified image of a pinhole was moved across the surface of the CCD in order to probe it's response at selected (sub-pixel) positions. The apparatus was established on an optical bench, for stability, and the details of the experimental set-up are presented below. During the course of the experiments we learnt how to improve our technique, and some comments on this are also given.

0-8194-1493-X/94/$6

2.2 The optical set-up

A projector housing was used as a light source; however we found it necessary to replace the original tungsten bulb with a halogen one in order to get a strong enough (blue) signal. We chose to use a 25 micron pinhole. The distance between the bulb and the pinhole was approximately 4 cm. An important component of the set-up was the use of a lens to demagnify the pinhole by a factor of ten, this resulted in a suitably small projected spot size at the CCD. The light-source and pinhole assembly could be moved on X, Y & Z micrometer-slides, whose motion was also demagnified by the fixed lens, so as to give a high precision of positioning at the CCD.

Narrow band colour filters (supplied by Oriel) were used to define the wavelengths of each measurement. Details of their bandwidths (defined as the full-width at half maximum, FWHM) and Transmissions are given below:

Wavelength (nm)	402	502	601	702	803	901
FMHM (nm)	9.7	10.5	10.0	9.2	9.4	11.1
Max. Transmission (%)	52	66	70	62	59	62

Table 1. Optical filter characteristics.

A 25 micron diameter pinhole, with a demagnifying ratio of 10:1, gives a theoretical spot size of 2.5 micron diameter (about 10 times smaller than the usual CCD pixel size). The X and Y micrometers mounted on the projector allowed a 10 micron step movement of the pinhole, which corresponds to a 1 micron movement of the light spot projected onto the surface of the CCD.

We found it necessary to use two different lenses in order to cover the entire spectral range. For the 500-900 nm range we used a high quality multiple lens (Pentax A 28-80), but this had a surprisingly low transmission factor in the blue. We then had to use a lower quality but blue-transmitting lens for the 400 nm measurements (Helios 40).

The cryogenic camera system (see following section) allowed operation of the detector at a controlled temperature. Figure 1 illustrates the complete experimental arrangement for the measurements described later.

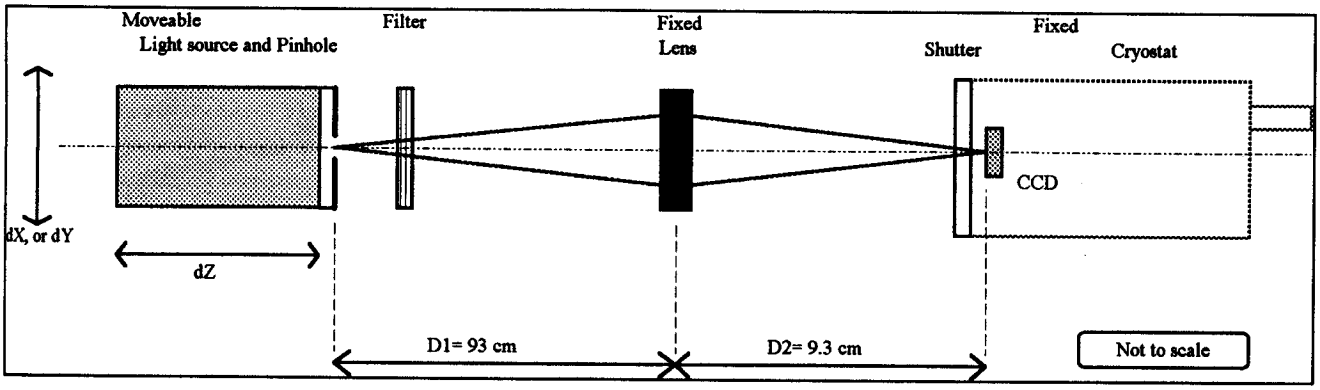

Figure 1. The experimental set-up for intra-pixel response measurements.

2.3 The CCD system.

The CCDs were operated by a 'standard' RGO CCD system:

A VME system provided us with full control of the CCD, and also provided various display and data-analysis tools. Full-frame images were taken for initial set-up, and subsequently small windowed frames were recorded. Intensity profiles were used to estimate FWHM, and hence allowed precise focusing. The image display tools allowed precise measurement, and repeatability of pixel locations; measurements being recorded in analogue-digital units (ADUs). Calibration tools allowed us to determine the conversion to electrons (e/ADU factor), when desired. Most exposures were of sufficient duration to ensure a good signal/noise ratio. At the beginning of each set of measurements (for each detector) the CCD read-out noise (and e/ADU factor) were determined. Three values were taken each time and averaged, the results are shown below. The

e/ADU conversion is also shown, together with operating temperature, and for later reference the pixel size of these three devices is also presented in table 2.

CCD	EEV 05-30	GEC P8603	Tek-1024
Readout noise (e^-)	5	31	9
electrons/ADU	0.8	1.9	1.2
Operating Temp. (K)	150	150	180
Pixel size (μm)	22.5	22	24

Table 2. Main operational parameters for the three CCDs used.

It should be noted that the noise figures here are above normal levels, since we did not optimise our controllers for these experiments; the S/N ratios were high, and readout noise was not a limiting factor.

2.4 Measurements of spot size

Since camera lenses are usually optimised for the centre of the visible spectrum (around 530 nm), we had to consider the possible alteration of the spot size due both to the optical aberration and to the imperfections of the set-up (misalignment of the lens inducing a coma, influence of the aperture and inner reflections in the lens). The three main phases of the spot size measurement are described below:

- We first used a large (1 mm diameter) pinhole in order to align the whole ensemble {projector, lens, camera-head}. We focused the CCD and measured the precise demagnification- which turned out to be 9.95 (nominally 10); for example, the 100 micron projected spot on the GEC P8603 CCD corresponded to a 4.57 pixel diameter. Figure 1 (above) showed this general arrangement.

- Next we installed the 25 micron pinhole. A microscope was put in place of the CCD camera-head. The microscope gave a much enlarged image of the spot, which was aligned and focused visually; a X40 objective together with an eyepiece was used here.

- The eyepiece was removed, and the CCD replaced at an extended distance behind the microscope, with a measured magnifying ratio of 1:155; a magnified image of the pinhole was therefore projected onto the CCD. For example, a 2.5 micron nominal projected spot was magnified to a size of 388 microns, which the CCD could measure precisely. The measurements were repeated for each wavelength. Figure 2 shows this spot-checking setup.

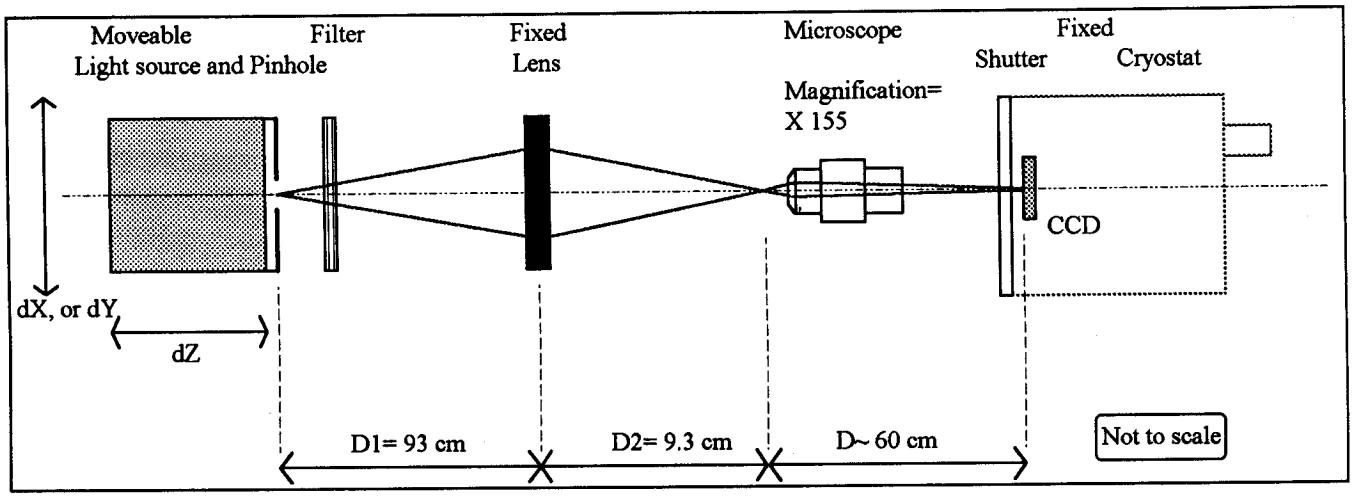

Figure 2. Optical arrangement for measuring the pinhole projected size.

The results of our spot measurements are shown below in table 3.

Wavelength (nm)	400	500	600	700	800	900
FWHM in X (μm)	4.5	2.8	2.8	3.3	3.7	4.3
FWHM in Y (μm)	4.4	2.5	2.6	2.8	2.9	3.4

Table 3. Spot size measurements.

Finally, the microscope was removed and the CCD repositioned, and refocused at the position of the projected 2.5 μm spot. The larger size of the spot at 400 nm is due to the lower quality of the lens used at this specific wavelength. The experimental error on the measurement of the spot size, considering the uncertainties on the positioning of the different parts of the set-up, (implying an error on the value of the global magnifying factor) is below 5%.

2.5 Measurement procedure

The initial set-up, and subsequent measurement sequences, will now be described: We initially focused the light spot onto the CCD (the adjustment of the focus was repeated at each wavelength), and checked both the alignment of the lens and the camera-head.

An exposure time was selected in order to have a high signal-to-noise ratio (the signal was generally above 20000 ADUs), and the spot position was adjusted in X and Y in a central region of the CCD, free of any cosmetic defects. The initial intra-pixel position was chosen in order to give a maximum peak signal; sometimes this was not exactly the case, but nevertheless all scans had a well-defined (repeatable) starting point.

Two scans were then performed: first in the X direction over a span of three pixels; the spot was then returned to its original position and a similar scan was performed in the Y direction. At each step position within the scan an exposure was taken; typically 10 sample steps per pixel were used.

For some wavelengths the process was repeated in order to estimate both the noise level and the precision of the positioning. The duplicate scans were found to be almost identical to the first, and after subtracting the two we derived a rms (root mean square) standard deviation of less than 2% of the mean, indicating an excellent repeatability and a good signal to noise ratio. In the plots presented later, the size of the plot symbols approximates the magnitude of this 'error'.

At selected wavelengths (500 nm, 700 nm and 900 nm for the GEC P8603 and the TEK 1024) we performed a complete 2 dimensional matrix of samples over a single pixel: the spot was moved in a 3 micron grid of points (8x8 samples) to entirely cover the pixel. At each position an exposure was taken and the image subsequently analysed.

For each image the signal intensity was measured within a 3 by 3 group of pixels centred on the spot; less than 2% of the signal was found outside this central area. The maximum signal in the central pixel constitutes what we call the '*peak*' signal, whereas the sum of the 3x3 centred group of pixels corresponds to the integrated signal, which we call the '*total*' signal. Table 4 illustrates a typical set of 7*7 pixels centred around a spot image. We also measured the signal in an annulus outside the 3*3 group (shown in bold below), in order to estimate the dark current/background level; this background level was always subtracted from peak and total measurements.

1026	1002	1004	1034	1036	1058	1046
1028	**1034**	**1018**	**1180**	**1094**	**1012**	1114
1054	**1026**	1195	2028	1154	**1028**	1206
1014	**1040**	2742	52486	1372	**1034**	1044
1022	**1062**	1730	3082	1222	**1054**	1064
998	**1023**	**1076**	**1062**	**1078**	**1002**	1054
1032	1030	1028	1023	1018	1018	1028

Table 4. A 7 by 7 group of pixels, measured with the GEC P8603 at 500 nm.

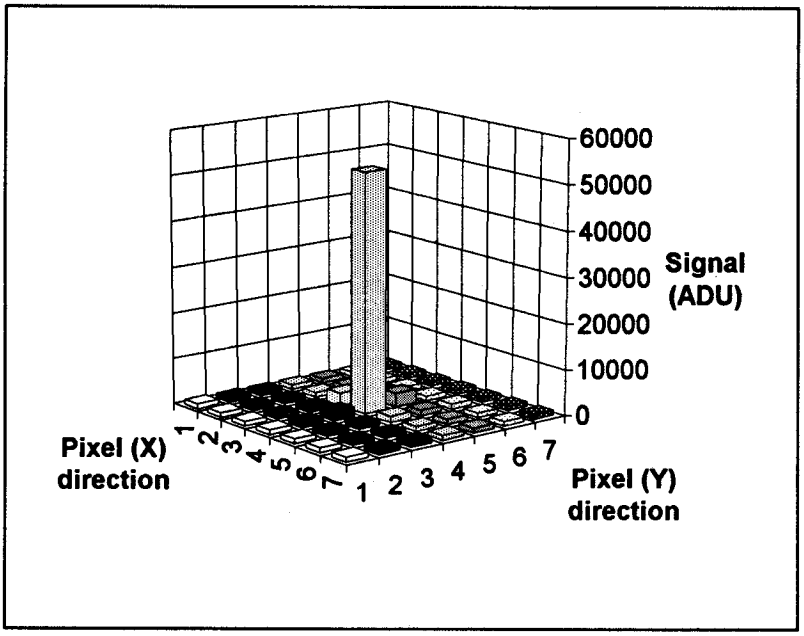

When the light spot is centred on the pixel, most of the signal falls in one pixel, with only a small percentage in the adjoining ones. When the spot falls on a pixel boundary, the signal is divided between two pixels, and their neighbours collect a very small additional signal. Figure 3 graphically illustrates the intensity distribution surrounding the central peak; the data is the same as table 4.

Figure 3: A block diagram of the 7 by 7 pixel grid centred on the spot.

2.6 Comments on future experiments

In the course of performing these experimental measurements we have identified several refinements which we would recommend for future use; these are listed below:

- Remove any effects due to light-source temporal changes. We used a stable power supply for the light source, and regularly checked it; the repeatability (of multiple identical scans) also gave us confidence in this. However, any 'accidental' temporal variation of light intensity will modulate the signal, and would be difficult to isolate from true spatial position modulation. A simple way to solve this problem would be to use a double-pinhole mask; one could then measure the small '2.5 micron' light spot at the same time as a larger (100 micron) spot. The latter signal, covering several pixels, would therefore be independent of any possible intra-pixel variation of the total signal- it could be used to scale the total light flux if necessary.

- Improve spot quality. As the accessible structure details are limited by the size of the projected spot, improving the lens quality would allow the projection of smaller light spots onto the surface of the CCD, limited ultimately by diffraction.

- Use one lens for all wavelengths. Finding, and using one lens, of high throughput and optical quality at all wavelengths would produce a better data set.

- Improve X & Y scanning precision. We took some care to align the CCD with the scanning directions, but in trying to analyse some of the observed features we have concluded that good confirmation of precise alignment would allow us to deduce a little more about the intra-pixel structure.

3. THE MEASUREMENTS

3.1 Introduction.

Here we will describe the set of measurements made, and then present representative results and a summary. It will not be appropriate to show the full set of data in this paper. The analysis of the measurements will be made in the next section. As discussed earlier, two types of results were available: the *peak* and the *total* signal. The former is a direct measurement of

the quantity of signal generated in the pixel on which the spot is focused and of charge sharing between adjacent pixels. "Ideally" this value should be maximum when the spot is centred on a pixel, and minimum (divided by four) when the spot is located at the intersection of four pixels. The *peak* signal can therefore be used as an indicator of the spot position inside a pixel (however, as we will see later on, care must be taken in interpretation of this). In addition, the *total* (or integrated) signal measures the actual detectivity (or sensitivity) of the device as a function of the intra-pixel spot position and is the relevant parameter in the study of the sub-pixel variation of response.

In all that follows X refers to the direction perpendicular to the channel stops, and Y to the direction parallel to the channel stops. In all the plots, the signal level is indicated in analog digital units (ADU), corresponding to the number of electrons collected divided by the gain-factor.

3.2 Coated GEC P8603

The GEC P8603 is a front-side illuminated 385x576 elements image sensor with a buried-channel and epitaxial structure. It has three electrodes per pixel and a frame transfer structure (the structure will be discussed in more detail in following sections). The device used in the experiment had been overcoated with a thin layer of fluorescent dyes (by ESO, see Cullum et al, 1985), and is equivalent to those used on our ING telescopes. We chose a 2 μm step for the X and Y scans, in order to have an integer number (11) of sample points within each 22 μm (square) pixel.

Spot scans were made at each wavelength (400-900 nm), in both X and Y directions. We measured this device first, and then refined our technique slightly for the other CCD measurements. Since the P8603 is very similar to the EEV-05-30 device, we will only show the latter results in this paper.

3.3 Uncoated EEV-05-30

The EEV 05-30 has mainly the same structure as the GEC P8603: it is also a front-side illuminated, epitaxial, buried channel, three phase CCD. The format is 1242*1152 pixels- but now with a 22.5 μm pixel size. For this device we used a 2.5 μm step , yielding 9 samples per pixel, for our X & Y scans (spanning 3 pixels in total). We also performed some Y scans with a 1μm step, over a single pixel, in order to determine the finest details of the structure. Another important difference was that the EEV 05-30 tested did not have any fluorescent dye coating; we therefore measured in that case the intrinsic response of the device.

In order to illustrate the data, we show here scan plots at 500 & 800 nm in the X & Y directions. The plots show how the peak, and total, signals vary with position at two different wavelengths.

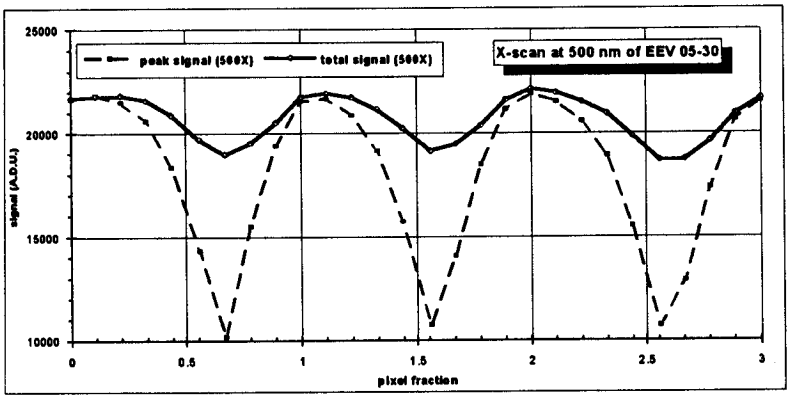

Figure 4. X-direction profile of EEV 05-30 at 500 nm.

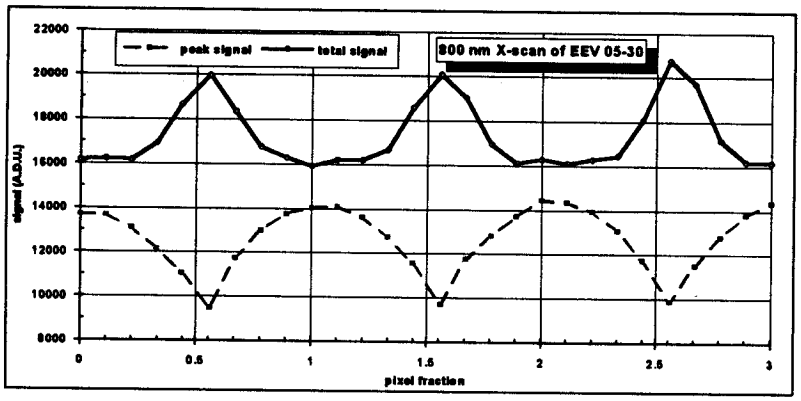

Figure 5. X-direction profile of EEV 05-30 at 800 nm.

The position of minimum *peak* signal, on each plot, identifies the channel stop location (where charge is divided between two pixels). It can be seen that at 500 nm the *total* measured response is a minimum at this location, whereas at 800 nm the *total* response is now a maximum.

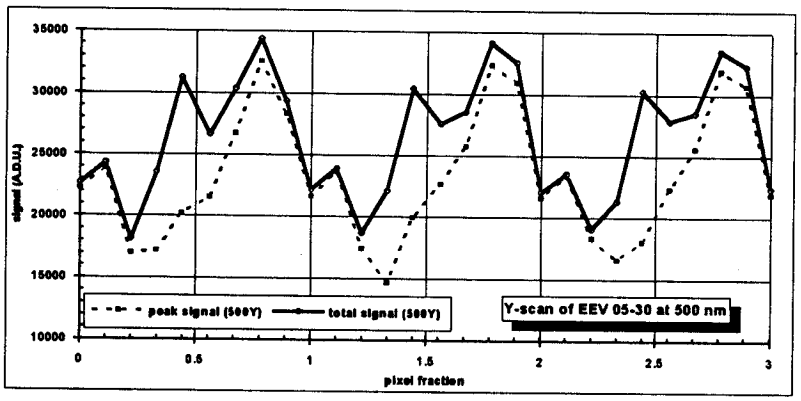

Figure 6. Y-direction profile of EEV 05-30 at 500 nm.

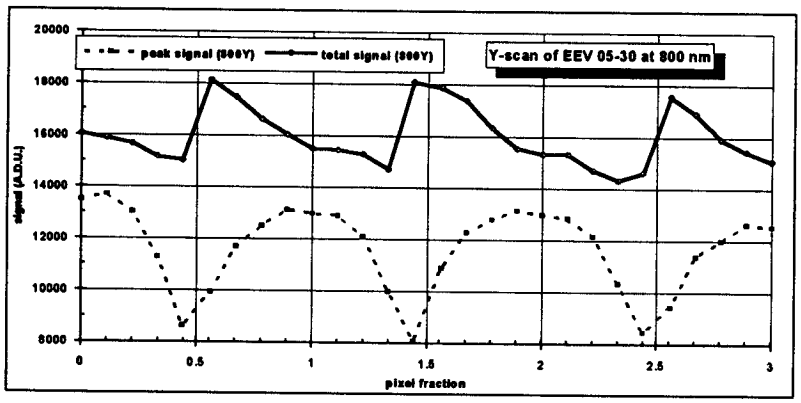

Figure 7. Y-direction profile of EEV 05-30 at 800 nm.

In the column direction the profiles are more complex, as expected for the triplet electrode structure. The minimum *peak* signal indicates the boundary between two pixels, although this is somewhat arbitrary since it depends on which electrodes we choose to keep at a high or low voltage. Indications of the triplet structure are seen at the shorter wavelength. Once again the *total* signal changes considerably with wavelength. We note that the modulation of *total* signal response is of order 50% at 500 nm.

In summary, it is clear that the sensitivity of the device is a clearly defined function of sub-pixel position at all wavelengths. Figure 8 presents a two-dimensional profile of the measured total signal at 500 nm.

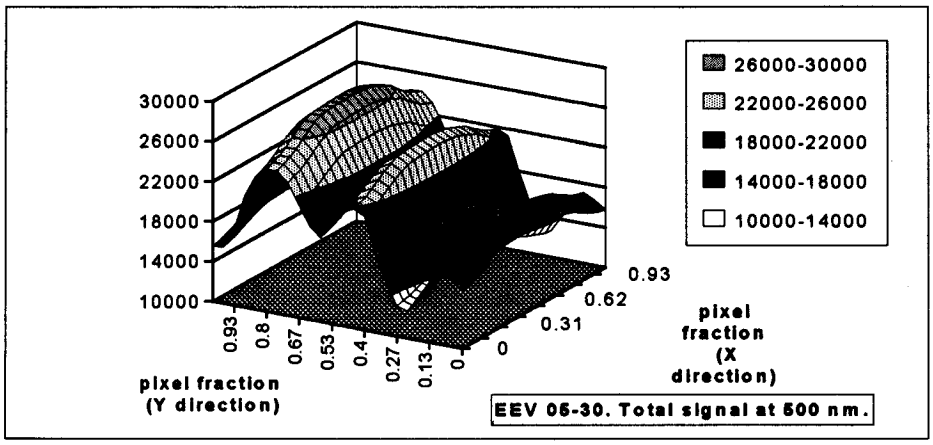

Figure 8. Two-dimensional plot of total signal response of EEV 05-30, at 500 nm.

3.4 Tek-1024 thin

The Tektronix 1024 is a back-side illuminated charge-coupled device, also fabricated using a buried channel, three phase electrode structure. The thickness of the silicon substrate is about 15 μm, and its back-face has an anti-reflection coating. The back surface has also received an enhancement treatment to reduce the recombination of carriers photo-generated near the surface (but as those treatments are uniform across the surface they should not affect the sub-pixel response). For this device we reverted to a 2 μm step, allowing 12 samples per pixel, for our X and Y scans.

We present below scans at 500 and 800 nm, in the X and Y directions of this device.

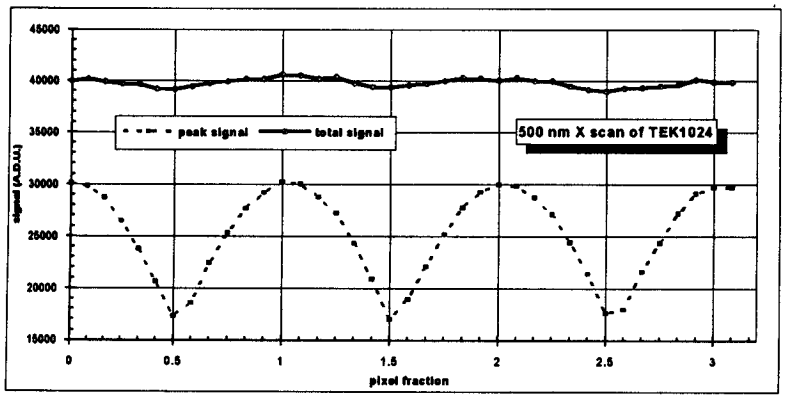

Figure 9. 500 nm X-scan of TEK1024.

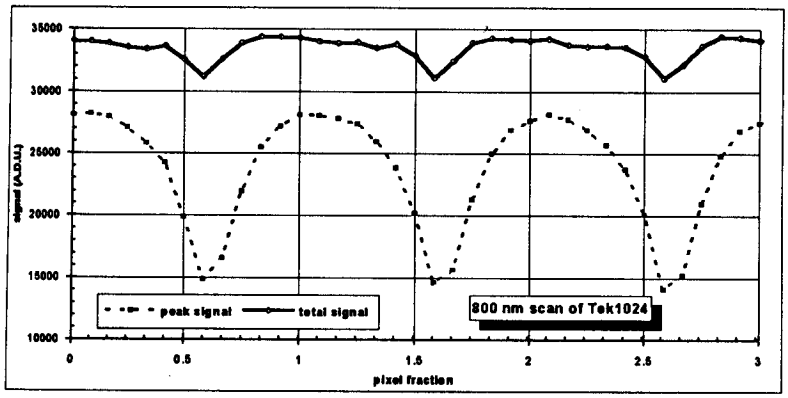

Figure 10. 800 nm X-scan of TEK1024.

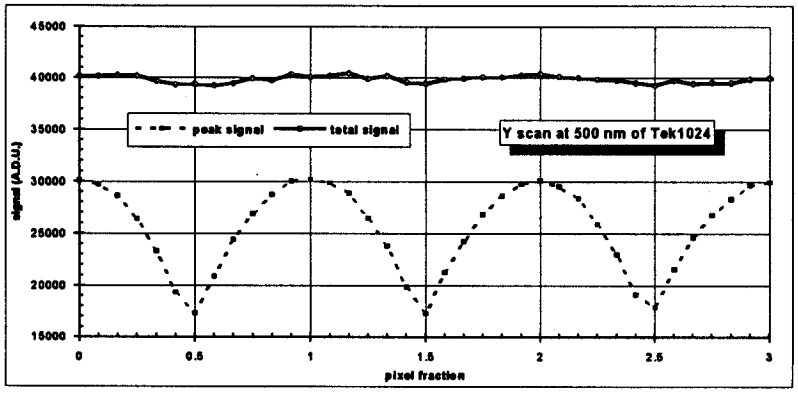

Figure 11. 500 nm Y-scan of TEK1024.

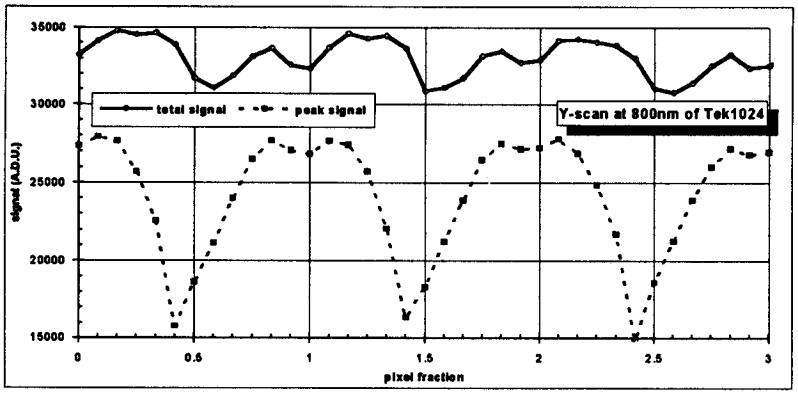

Figure 12. 800 nm Y-scan of TEK1024.

In all plots, the minimum *peak* signal again indicates the positions of pixel boundaries. Modulation of *total* signal response is seen in both directions at all wavelengths. The modulation at shorter wavelengths is somewhat unexpected, with this backside-illuminated thinned device (see later discussion). The shape of the modulation varies quite strongly with wavelength.

4. MODELS OF THE CCD STRUCTURE

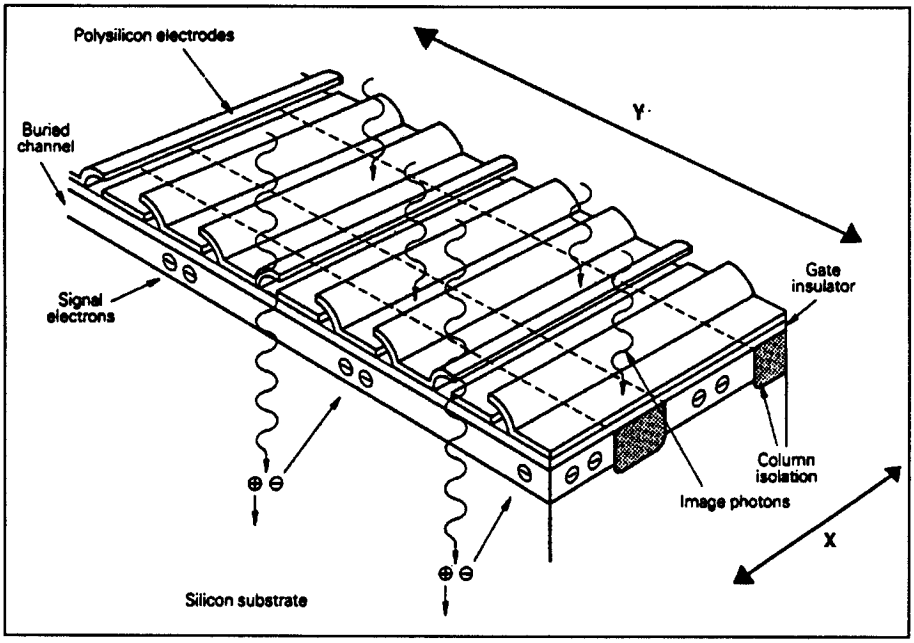

In order to interpret the results we need to examine the CCD pixel structure, although we shall not attempt to fully explain how a CCD operates. Figure 13 shows a section through a typical CCD; figure 14 gives a representation of the electrode layers of a 3-phase, 3-level electrode device; whilst figure 15 gives a plan view of a pixel showing the four main components of a pixel.

Figure 13. Section of a buried channel CCD image sensor. The picture illustrates three pixels in the Y direction and shows the channel stop structure (column isolation) in the X direction. (from Burt, 1982).

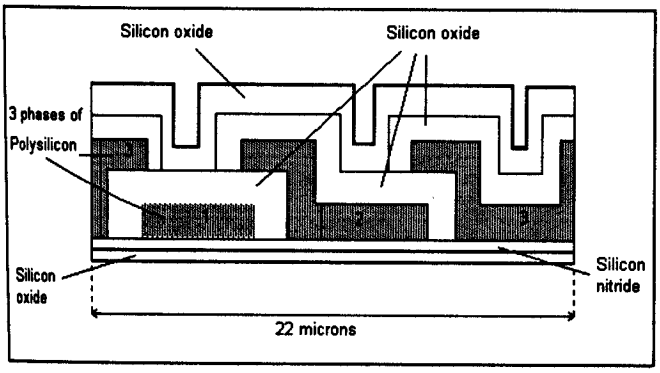

Figure 14. The surface (frontside) layers of a GEC P8603 in the Y direction (not to scale). The various layers range in thickness from 85-500 nm nominally. Note that up to 7 layers are present.

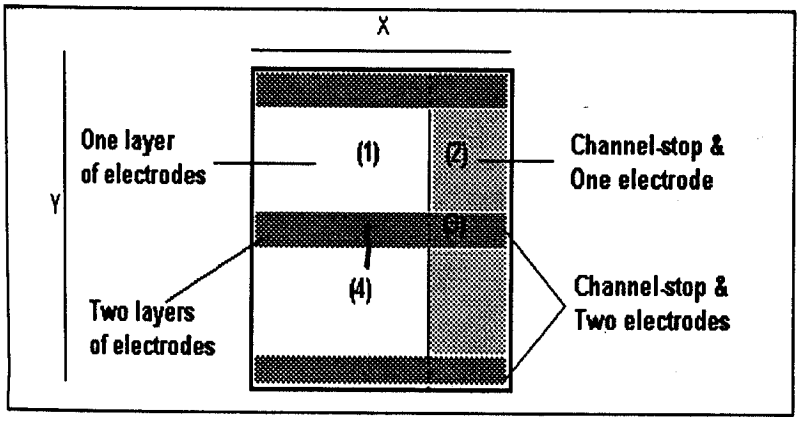

Figure 15. Plan view of pixel, showing four main regions of electrode structure.

The GEC and EEV devices are 'normal' frontside illuminated sensors, in which the photons pass through the electrodes before reaching the active region. Only photons that are absorbed within this active region generate charges which constitute the image signal. The active region is defined by a depletion region under the active electrodes; the depth of this region is typically 5-10 microns.

The Tek device is an example of a thinned, backside-illuminated device, in which the photons can reach the depletion region more directly from the rear-surface. This eliminates the absorption loss of the electrodes and yields higher responsivity.

All types of CCD have a multilayer electrode structure, and the diagrams above show this detail schematically. The electrodes confine and control the charge in the Y-direction, whilst an implanted strip (the channel stop) defines each pixel in the X-direction. The electrodes overlap, and this results in regions of 'single' and 'double' electrode thickness, separated by insulating layers. Each pixel has a precise internal structure which is replicated within every pixel of the device.

Further details of CCD structure may be found in the following references: Burt (1982), Howes & Morgan (1979), Janesick & Elliott (1984), McLean (1989), Opt Eng (1987). The EEV device was described by Pool et al (1990). The Tek device has been discussed by Marsh et al (1991), and Blouke et al (1991).

5. DISCUSSION OF RESULTS

5.1 Introduction

In this section we will attempt to explain the main features that we have observed in the measurements of signal response as a function of intra-pixel position, and wavelength. As an introduction we initially list below the main elements that we believe influence the response:

The electrode structure. The multiple overlapping levels of the triplet electrodes create a multilayer structure. The layers are of comparable thickness to our 'optical' wavelengths, and so we should expect interference as well as absorption effects. Each of the three electrodes is about 7 μm wide, with a 2 μm overlap (approximately).

The channel-stop barrier. This highly doped region acts as a barrier between pixels in the X-direction. It might be expected to have different optical and electrical properties, hence influencing the response nearby. In addition the surface layers above it may differ. The optical properties of heavily doped silicon have been discussed by Jellison et al (1981), and Lubberts et al (1981). In the case of the GEC device, with 22 μm pixels, the channel stop is nominally 6 μm wide.

The depletion region. The photo-generated electrons are contained within a region of electric field (depletion region) under the active electrodes; these are also known as potential wells. Typically, for normal resistivity silicon, the depletion depth is of order 5 μm. Essentially all charges generated in this region are collected, whereas charges generated outside it suffer a lower probability of collection. The collection rate depends on probability of diffusion, which is a function of depth (wavelength) and of X/Y position.

Thin, backside-illuminated structure. In this case the electrodes should not have such a primary role in contributing to photon loss. However, as we shall discuss, their structure is still very evident in the intra-pixel response pattern. If the device is made quite thin, then the device thickness matches the depletion depth and most charges can be collected. However, if the device is too thin, then longer wavelength photons have a poor absorption within the device.

5.2 The influence of the regions.

The complex electrode structure might be expected to give a change in transmission with intra-pixel position; this is also a function of wavelength. Superficially this could be expected to account for the general nature of the spectral and spatial response of the CCD. However, we observe quite dramatic changes in the nature of the intra-pixel profiles as the wavelength changes. In fact, with a knowledge of the thickness of the electrode layers, it is clear that multi-path optical interference plays an important role in defining the optical response.

The channel-stop region might merely be considered as a 'dead' barrier within the CCD; this is not so. The channel stop depth is of order 1 μm , hence short-wavelength light does generate charge within this shallow region, which recombines rapidly and is lost. However, longer wavelengths generate charge deeper within the silicon, and this can diffuse sideways and be collected; the loss of response therefore depends on wavelength. In addition, the EEV/GEC devices have a variation in surface thickness over the channel stops, and so the nature of the optical absorption and interference can change. A discussion of charge diffusion may be found in Hopkinson (1983), Hopkinson (1987), and Blouke et al (1991).

We have obtained data about the structure of the P8603 CCD (Burt, 1993), and together with silicon refractive index data (Aspnes, 1987), used it to calculate the optical transmission through the electrodes (using 'FilmCalc' programme). A simple analysis is made more complex due to variations of manufacturing tolerances which mean that the layer thicknesses are not precisely known; thickness variations in silicon oxides have been analysed by Lee et al (1985). Consequently we calculated the transmission for a set of combinations (0, ± 5%, ± 10 % of nominal thickness of each layer) and then derived a mean figure, for each of the four regions within a pixel (shown in figure 15).

The absorption depth of silicon is a strong function of wavelength; this leads to loss of sensitivity at long wavelengths since photons pass straight through the depletion (active) region. The charge collection efficiency is therefore a function of wavelength (depth) and lateral position (depending on whether the charge is generated under a depletion region or not).

A model of the device response, for each of the four different regions, was obtained by combining 'electrode' transmission with charge collection efficiency. By combining the response of each region, weighted according to its estimated area, we derived a model of the global quantum efficiency response of a GEC CCD. The model corresponded with the measured response to within 10% over the range 500-1000 nm, and this excellent agreement gave us good confidence that our calculations were realistic.

The backside illuminated structure might be expected to exhibit very different characteristics. Short wavelength photons should be absorbed directly, without any influence of surface (frontside) structure; a more uniform response is expected. Longer wavelength photons do penetrate a significant fraction of the depletion depth, and so effects due to the shape of the depletion region might be expected. Furthermore, photons that reach the frontside can then suffer optical interference; long wavelength *fringes* are evidence of multiple path reflections within the CCD.

5.3 Explanation of features seen in our measurements.

As stated above, the measurements of *peak* signal indicate relative position within the pixel, due to charge sharing effects. As expected, the *peak* signal modulation is close to 50% in some cases; at longer wavelengths the modulation is lower due to deeper absorption, and greater diffusion effects.

The *total* signal response is seen to vary with X-position within the pixel. We attribute this to the lower sensitivity of the 'dead' channel stop and to variations in optical interference above it (compared to the rest of the pixel). Note that the 800 nm response of the EEV device is actually **enhanced** above the channel-stop- this clearly demonstrates the dominant effect of optical interference in determining the response.

Interestingly, even the thinned Tek device exhibits X-modulation in response at short wavelengths (~4% at 500 nm). We believe this is due to the influence of the depletion region, or rather the lack of it below the channel-stop. Short wavelength photons generate charge near the rear surface (500 nm photons within 3 micron), and hence well away from the front surface electrodes or channel stop. We therefore assume that the measured variation in response is due to the non-uniform nature of the depletion region, which influences charge collection efficiency. We also observed that the *total* response was not a minimum under the channel stop , at the longest wavelength (900 nm). We suspect that the structure must be more complex in the X-direction than that of a simply defined channel.

In the Y direction all devices exhibit a response that is a function of position relative to the electrodes. As expected, the effects are very pronounced at short wavelengths for the frontside illuminated devices. Clear evidence of the influence of the electrode structure is seen. The patterns change strongly with wavelength, again underlying the importance of optical interference effects.

The thinned Tek device also exhibits modulation in Y-response at short wavelengths; we similarly attribute this to the effects of the depletion region (which only exists under the active electrodes). The amplitude is quite small (<2%) at 500 nm. Only at wavelengths beyond 700 nm can detail of the electrode structure be seen; modulation of *total* signal can exceed 10%.

The good repetition of repeated scans shows that intra-pixel structure is very similar, at least for adjacent pixels and probably for all pixels, within a device.

6. COMPARISON WITH SOME UNDERSAMPLED DATA

We have seen that the measured variations of signal within a pixel are not negligible; however, in practice, this problem will only occur in specific circumstances: when the image of the observed object on the CCD is smaller than the size of a pixel, and when the spectral bandwidth is limited . The variation will be most pronounced when both conditions are true. The first condition arises from spatial undersampling (in case of very good seeing conditions for instance), and the second can occur during observations through colour filters (in photometry), or spectroscopy.

We were prompted to examine the problem of sub-pixel non-uniformity of sensitivity following some observations made with the Faint Object Spectrograph (FOS-1) in June 1992, at the Isaac Newton Telescope on La Palma Observatory (see Rutten, Dhillon, & Horne, 1992; referred to as RDH below).

The FOS instrument yields a low dispersion spectrum with approximately 1.2 arcsecond/pixel. The primary dispersion is in the column direction, but internal cross-dispersion has the effect of causing the spectrum to curve across several columns. RDH recorded spectra in conditions of sub-arcsecond seeing and found unexpected periodic features in their spectra when

analysed. At first these were attributed to poor data extraction and re-sampling effects, but we now understand that the internal intra-pixel response of the CCD was responsible. Figure 16 illustrates an example of such an extracted FOS spectrum, taken in conditions of 0.8 arcsecond seeing; the ripples are clearly visible at most wavelengths.

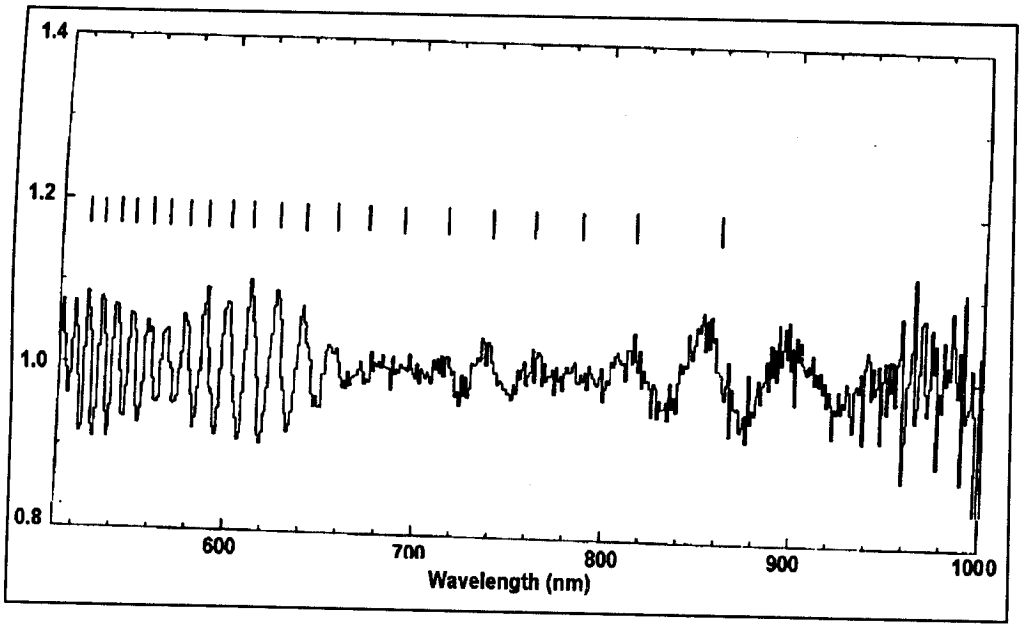

Figure 16. Extracted, normalised FOS spectrum, bringing out the relative amplitude of the 'undersampling ripples'. The marks above the spectrum indicate where the spectrum crosses the centre of a column. (From RDH 1992).

We convolved a 'seeing' Gaussian of 0.8 arcsec (0.67 pixel-width) with our measured intra-pixel *total* response and found that it reproduced the nature of the ripples quite well. The change in frequency of these ripples is due to the increased curvature of the spectrum at blue wavelengths, causing it to cut across the columns more rapidly. It can be seen that the amplitude (and phase) of the ripples changes with wavelength; we believe this is due to the fact that the intra-pixel response, at a given intra-pixel position, changes with wavelength (e.g. the response over the channel stop may be enhanced or reduced depending on wavelength).

The purpose of the above example was merely to illustrate that intra-pixel response variations introduce genuine effects in CCD data. A fuller discussion of the above data can be found in the references (RDH, Jorden et al (1993), & Dhillon et al (1993).

7. SUMMARY AND CONCLUSIONS

We have presented here the results of some intra-pixel sensitivity variation measurements for three different charge-coupled devices: two front-side illuminated (the GEC P8603 and the EEV 05-30) and one back-side illuminated (the Tektronix 1024). These results have underlined the dramatic importance of the detector sub-pixel structure on its response when illuminated by a light spot smaller than the pixel size. The analysis of the experimental results and a simple modelling of a front-side device have shown that the main reason for those variations could be attributed to the optical interferences within the surface layers of the device (e.g., the electrode structure) . The change in optical absorption as a function of material layer and depth also contributes substantially to the variation of the response, as well as the channel-stop structure and the field distribution within the device (especially for the back-side illuminated CCD).

In conditions of spatial undersampling, we believe that these effects can influence data in several areas of astronomical observation: spectroscopy, photometry and astrometry. Features in spectroscopic data were discussed above, the influence on photometry is straightforward, and clearly position-determination to sub-pixel accuracy (for astrometry or star-tracking/ centroiding purposes) can be influenced. Hence, the sub-pixel variation of response, though generally assumed to be unimportant, can have a non-negligible effect and should be considered at least at the time of data analysis. However, as an

analytic model of the intra-pixel sensitivity is complex and would have to be reconsidered for each type of device, the detailed analysis of undersampled spectra or images might be a real problem. It would therefore be prudent, as far as possible, to adopt an appropriate 'sampling strategy' during the observation in case of a non-fully sampled signal, especially if narrow-band filters are used.

We should emphasise that all of our laboratory measurements were taken with very small (~2 micron) sampling spots; this allowed us to determine the intra-pixel response quite precisely. In reality, we assume that most observations will be taken with much larger image sizes, and the effect of intra-pixel response will be diminished accordingly. For example, with a ratio **R= 0.8** (image FWHM/pixel-size, Buonnano & Iannicola, 1988), **we should expect a modulation of response of a few percent**, depending on where precisely the image falls within the pixel.

To emphasise the nature of these intra-pixel response modulations we conclude by showing contour maps of total signal response at two wavelengths, for the Tek CCD; see figures 17 and 18 below. A strong repeatable pattern is seen, whose nature changes quite strongly with wavelength, for reasons discussed above.

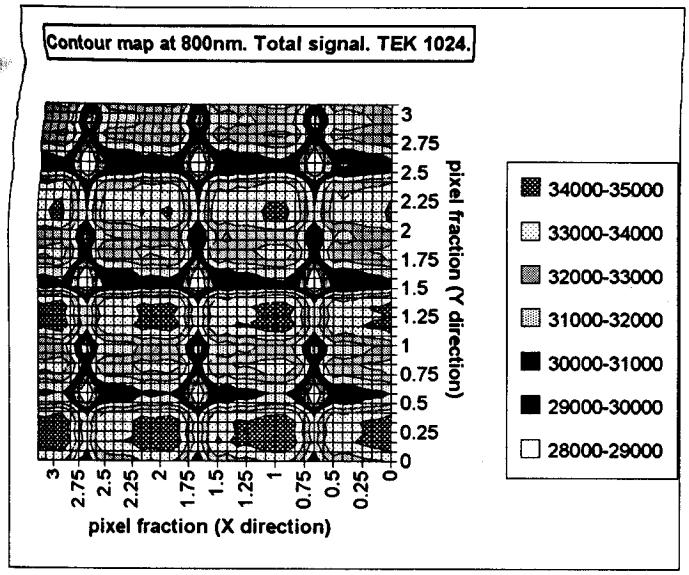

Figure 17. Two-dimensional contour map of Tek CCD total intra-pixel response at 800 nm.

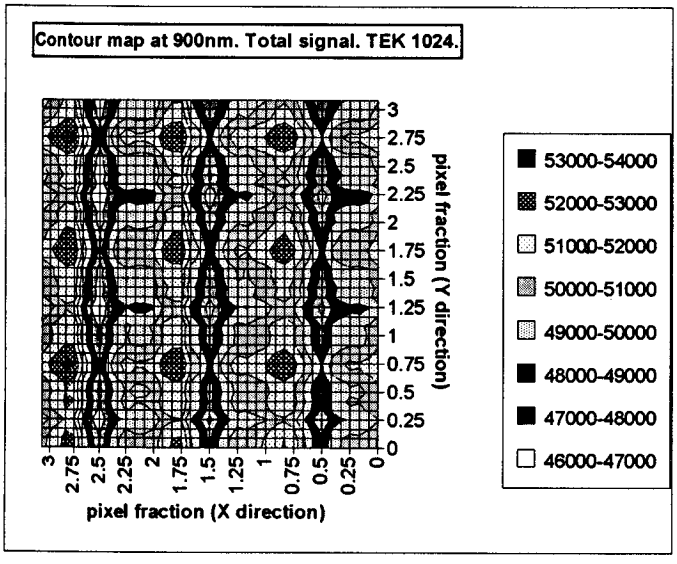

Figure 18. Contour map of Tek CCD intra-pixel response at 900 nm.

In conclusion, we will summarise below our main findings:

- Response varies with intra-pixel position, in X & Y directions. Response is not necessarily highest at the 'centre' of a pixel.
- Response modulation varies strongly with wavelength, mainly due to interference effects.
- Response can be lower or higher at the channel stop positions, depending on wavelength
- Thinned devices exhibit small but finite response modulation, even at short wavelengths.
- Intra-pixel structure is stable and very repeatable, from one pixel to another

8. ACKNOWLEDGEMENTS

Some of this work was prompted by observations made by Vik Dhillon and colleagues, and we thank him for several useful discussions. We appreciated the assistance given by Sue Worswick in the setting up of the optics for the experiment. We also had very useful discussions and information from David Burt (GEC Hirst Research Centre) on the architecture and performance of GEC/EEV devices.

9. REFERENCES

Aspnes D E, 1987, *Optical Functions of Intrinsic Silicon,* EMIS Datareview RN=17801.
Blouke M M, Delamere W A, Womack G, 1991, Proc SPIE **1447**, 142.
Burt D J, 1982, EEV (GEC) Technical Note 1. See also more recent EEV Technical Notes on CCDs.
Burt D J, 1993, private communication.
Cullum M, Deiries S, D'Odorico S, Reiss R, 1985, Astr. Astrophys, **153**, L1.
Dhillon V, Rutten R, Jorden P R, 1993, RGO Gemini. **41**,7.
FilmCalc, FTG Software Associates, PO Box 579, Princeton, NJ 08542.
Hopkinson G R, 1983,. Nuclear Instruments and Methods, **216**, 423.
Hopkinson G R, 1987, Optical Engineering, **26**, 8.
Howes M J, Morgan D V, 1979, *Charge-Coupled Devices and Systems,* Wiley.
Janesick J R, Eliot T, 1984, Proc SPIE, **501**,2.
Jellison G E, Modine F A, White C W, Wood R F, Young R T, 1981, Physical Revue Letter. **46**, 1414.
Jorden P R, Deltorn J-M, Oates P, 1993, RGO Gemini, **41**, 1.
Lee T -H et al, 1985, Trans IEEE, **ED-32 (8)**, 1439.
Lubberts G, Burkey B C, Moser F, Trabka E A, 1981,. Journal of Applied Physics, **52**, 6870.
Marsh H H, Hayes R, Blouke M M , Yang F H, 1991, Proc SPIE, **1447**, 298.
McLean I S, 1989, *Electronic and computer-aided astronomy*, Ellis Horwood.
Optical Engineering, 1987, **26**, parts 7, 8 & 9. Many CCD papers.
Pool P J, Suske W A F, Ashton J E U, Bowring S R, 1990, Proc SPIE, **1242**, 17.
Purll D J, 1978, *Development study for a high accuracy star sensor*, Vol. 3, SIRA study for ESA, ESTEC Ref 2454/75.
Rhutton R, Dhillon V, Horne K, 1992, RGO Gemini, **38**, 22.
Wright J F, 1982, *The application of imaging charge-coupled devices in astronomy*, PhD Thesis, Univ. of Cambridge, UK.